Higher-order exceptional points in a non-reciprocal waveguide beam splitter

Hamed Ghaemi-Dizicheh[1],* Shahram Dehdashti[2], Andreas Hanke[1], Ahmed Touhami[1], and Janis Nötzel[2]

[1]*Department of Physics and Astronomy, University of Texas Rio Grande Valley, Texas 78539, USA*

[2] *Emmy-Noether Group Theoretical Quantum Systems Design, Technical University of Munich, Munich, Germany*

Non-Hermitian systems have attracted significant interest because of their intriguing and useful properties, including exceptional points (EPs), where eigenvalues and the corresponding eigenstates of non-Hermitian operators become degenerate. In particular, quantum photonic systems with EPs exhibit an enhanced sensitivity to external perturbations, which increases with the order of the EP. As a result, higher-order EPs hold significant potential for advanced sensing applications, but they are challenging to achieve due to stringent symmetry requirements. In this work, we study the dynamics of a generalized lossy waveguide beam splitter with asymmetric coupling by introducing non-reciprocity as a tunable parameter to achieve higher-order EPs even without dissipation. Using the Schwinger representation, we analytically derive eigenvalues and numerically demonstrate the formation of EPs. Moreover, we analyze the evolution of NOON states under activated non-reciprocity, highlighting its impact on quantum systems. Our results open new pathways for realizing higher-order EPs in non-reciprocal open quantum systems.

I. INTRODUCTION

In recent years, non-Hermitian systems have attracted significant attention due to their distinct properties such as non-Hermitian edge states [1, 2] and transport effects [3, 4]. In particular, non-Hermitian systems are characterized by the existence of exceptional points (EPs), where two or more eigenvalues and their corresponding eigenstates become degenerate [5, 6]. Among the unique properties of non-Hermitian systems due to EPs are topological transport phenomena [7–9], robust wireless power transfer [10], asymmetric mode switching [11], stopping light [12], loss-induced suppression and revival of lasing [13, 14], non-reciprocity [15], and enhanced classical sensitivity [16–18]. One of the most important properties of EPs in non-Hermitian systems is the sensitivity to changes in external parameters [17–19], which finds important applications in a wide variety of systems [7, 20, 21]. Since the singularity-enhanced sensitivity increases with the order of the EP, i.e., the number of degenerate eigenmodes, systems with higher-order EPs offer even greater promise for developing advanced sensors and precise measurement equipment required in diverse fields. To illustrate the origin of this high sensitivity, consider the eigenvalues of an arbitrary non-Hermitian matrix $M(\gamma)$ as a function of a parameter $\gamma \in \mathbb{C}$ with an n-fold EP at γ_{EP}. In the vicinity of γ_{EP}, different eigenvalues λ of $M(\gamma)$ are separated by a gap $\delta\lambda$ given by a series [22]

$$\delta\lambda = \sum_{j=1}^{\infty} c_j (\gamma - \gamma_{\mathrm{EP}})^{j/n} \, ,$$

where c_j are coefficients. The leading contribution of the derivative of $\delta\lambda$ with respect to γ in the vicinity of the EP is given by

$$\partial\delta\lambda/\partial\gamma \sim \frac{1}{(\gamma - \gamma_{\mathrm{EP}})^{1-1/n}} \, ,$$

which becomes singular at the EP since $n \geq 2$. This clearly shows a high sensitivity of the eigenvalue gap $\delta\lambda$ to the variation of the parameter γ away from the EP, which increases with the order n of the EP.

However, realizing higher-order EPs poses practical challenges across different platforms. The primary obstacle originates from the necessary fine-tuning of system parameters, which is required by a higher-order symmetry necessary for eigenmode degeneracy [23]. To overcome this challenge, waveguides are promising candidates [24, 25]. For instance, Quiroz-Juárez et al. realized higher-order EPs in a single, lossy waveguide beam splitter in the quantum domain [26]. To this end, they studied the dynamics of a lossy waveguide beam splitter within the post-selected N-photon subspace, where the creation of higher-order NOON states and number-resolving photon detectors is required instead of fine-tuning. In experimental systems, introducing dissipation while maintaining control over other parameters of the beam splitter can be challenging. Furthermore, engineering specific dissipation rates without incurring undesirable losses is difficult. Dissipation can also diminish interference effects, thereby limiting the efficacy of the beam splitter in applications such as interferometry or quantum state manipulation. To address these problems, in this study we consider a generalized version of a lossy beam splitter by introducing an asymmetric coupling between its waveguides. In classical systems, such non-reciprocal platforms have numerous applications including optics and photonics [27–29], electrical circuits [30, 31], and nonlinear topological models [32].

In this work, we explore the role of non-reciprocity in engineering EPs within a lossy waveguide beam splitter. By introducing non-reciprocity as an additional degree of

---

freedom, we demonstrate that it facilitates the emergence of higher order exceptional points without stringent dissipation requirements. Our analysis reveals that increasing non-reciprocity lowers the critical dissipation threshold for EP formation, and in the extreme case of a unidirectional system, EPs arise in the absence of dissipation.

The paper is organized as follows. In Section II, we derive the eigenvalues of a non-reciprocal, lossy waveguide beam splitter using the Schwinger representation approach and numerically study properties of the higher-order EPs for this system. We also demonstrate how altering the system's non-reciprocity affects the realization of EPs of order $N+1$ within the post-selected N-photon subspace. In Section III, we study the dynamical evolution of a NOON state both analytically and numerically by activating non-reciprocity in this system. Section IV contains our conclusions.

II. SPECTRUM OF A NON-RECIPROCAL, LOSSY WAVEGUIDE BEAM SPLITTER

We consider a non-reciprocal beam splitter with two coupled waveguides depicted schematically in Fig. 1. The Hamiltonian in second quantization is given by (using units such that $\hbar = 1$)

$$\hat{H} = \omega_0(\hat{a}^\dagger \hat{a} + \hat{b}^\dagger \hat{b}) + \nu \hat{b}^\dagger \hat{a} + \nu' \hat{a}^\dagger \hat{b} - i\Gamma \hat{b}^\dagger \hat{b}, \quad (1)$$

where $\hat{a}^\dagger$ (a) and $\hat{b}^\dagger$ (b) are bosonic particle creation (annihilation) operators for photonic modes in the two waveguides and Γ denotes the dissipation coefficient of the lossy waveguide. The coupling between waveguides a and b is given by ν and ν', and ω_0 is the on-site energy. A non-reciprocal waveguide beam splitter is obtained for $\nu \neq \nu'$. To reveal arbitrary-order EPs in the coupled waveguide beam splitter, we represent the Hamiltonian in Eq. (1) in the two-mode N-photon subspace. This subspace is spanned by $N+1$ orthonormal states $|\phi_m\rangle :=$ $|N-m, m\rangle = |N-m\rangle_a |m\rangle_b$ where $0 \le m \le N$.

The Hamiltonian in Eq. (1) commutes with the total photon-number operator

$$\hat{N} = \hat{a}^\dagger \hat{a} + \hat{b}^\dagger \hat{b}, \quad (2)$$

which implies that N is conserved. Based on the Schwinger representation [33], we introduce ladder operators $\hat{J}_+$, $\hat{J}_-$ such that

$$\hat{J}_+ = \hat{J}_x + i\hat{J}_y = \hat{b}^\dagger \hat{a}, \quad \hat{J}_- = \hat{J}_x - i\hat{J}_y = \hat{a}^\dagger \hat{b}, \quad (3)$$

which satisfy the SU(2) commutation relations. Expressed in terms of the ladder operators $\hat{J}_+$, $\hat{J}_-$, the Hamiltonian in Eq. (1) takes the form

$$\hat{H} = (\omega_0 - i\Gamma/2)\hat{N} + \nu \hat{J}_+ + \nu' \hat{J}_- - i\Gamma \hat{J}_z. \quad (4)$$
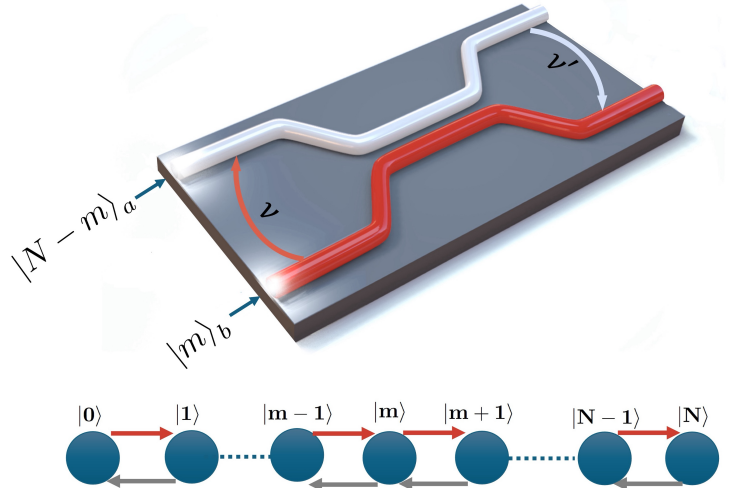

FIG. 1. Schematic of a non-reciprocal single, lossy, 2-leg waveguide beam splitter excited with N indistinguishable photons prepared in the state $|N-m, m\rangle = |N-m\rangle_a |m\rangle_b$ $(0 \le m \le N)$, where a represents the neutral (white) waveguide and b the lossy (red) waveguide.

The eigenvalues can be readily derived analytically by diagonalizing $\hat{H}$ in Eq. (4). To this end, we use the Baker–Campbell–Hausdorff formula and SU(2) commutation relations to obtain the following boosts (or rotations):

$$e^{i\theta \hat{J}_\pm} \hat{J}_z e^{-i\theta \hat{J}_\pm} = \hat{J}_z \mp i\theta \hat{J}_\pm, \quad (5)$$

$$e^{i\theta \hat{J}_z} \hat{J}_\pm e^{-i\theta \hat{J}_z} = e^{\pm i\theta} \hat{J}_\pm, \quad (6)$$

$$e^{i\theta \hat{J}_+} \hat{J}_- e^{-i\theta \hat{J}_+} = \hat{J}_- + 2i\theta \hat{J}_z - (i\theta)^2 \hat{J}_+, \quad (7)$$

$$e^{i\theta \hat{J}_-} \hat{J}_+ e^{-i\theta \hat{J}_-} = \hat{J}_+ - 2i\theta \hat{J}_z - (i\theta)^2 \hat{J}_-. \quad (8)$$

Since the Casimir operator of the system is given by $\hat{C} = (\hat{N}/2)(\hat{N}/2+1)$ it follows that the operator $\hat{N}$ commutes with all the generators of $SU(2)$. Consequently, using Eqs. (5) and (8), the Hamiltonian in Eq. (4) transforms as follows:

$$\begin{aligned} \hat{H}' &= e^{i\theta \hat{J}_-} \hat{H} e^{-i\theta \hat{J}_-} \\ &= (\omega_0 - i\Gamma/2)\hat{N} + \nu \hat{J}_+ + (\nu\theta^2 + \nu' + \Gamma\theta)\hat{J}_- \\ &\quad - i(2\theta\nu + \Gamma)\hat{J}_z. \end{aligned} \quad (9)$$

Setting

$$\theta = \frac{-\Gamma^2 \pm \sqrt{\Gamma - 4\nu\nu'}}{2\nu} \quad (10)$$

eliminates the third term (proportional to $\hat{J}_-$) on the right-hand side of Eq. (9). Using Eq. (5), the transformed Hamiltonian becomes

$$\hat{H}' = (\omega_0 - i\Gamma/2)\hat{N} - i(2\theta\nu + \Gamma)e^{-i\phi \hat{J}_+} \hat{J}_z e^{i\phi \hat{J}_+}, \quad (11)$$

where

$$\phi = \frac{\nu}{2\theta\nu + \Gamma}\,. \qquad (12)$$

By applying the similarity transformation $U\hat{H}'U^{-1}$, where $U = e^{i\phi\hat{J}_+}$, we can diagonalize the Hamiltonian $\hat{H}'$. The eigenvalues are then expressed in analytical form as

$$\lambda_r = (\omega_0 - i\Gamma/2)N \pm r\sqrt{4\nu\nu' - \Gamma^2}\,, \qquad (13)$$

where $r = -N, -S+1, \ldots, N$. Since in this reference frame the eigenvectors are expressed as $v_i = [\delta_{0,i}, \ldots, \delta_{0,N-1}]^T$, the corresponding eigenvectors of the Hamiltonian (1) are given by $e^{-i\theta}e^{-i\phi}v_i$.

To show the effect of non-reciprocity, we parametrize the coupling amplitudes ν, ν' such that

$$\nu = \nu_0(1 + \eta)\,, \qquad \nu' = \nu_0(1 - \eta)\,, \qquad (14)$$

where $0 \le \eta \le 1$ is the non-reciprocity parameter. By adjusting the non-reciprocal parameter η within the range $0 \le \eta \le 1$, the system transitions from a reciprocal configuration at $\eta = 0$ to a fully unidirectional coupled waveguide regime at $\eta = 1$.

According to Eq. (13), the adjacent eigenvalue difference, defined as $\Delta\lambda \equiv \lambda_r - \lambda_{r-1}$, is given by

$$\Delta\lambda = \sqrt{4\nu_0^2(1 - \eta^2) - \Gamma^2}, \qquad (15)$$

which is purely real when the dissipation coefficient satisfies $\Gamma \le 2\nu_0(1-\eta^2)^{\frac{1}{2}}$, and becomes purely imaginary for $\Gamma > 2\nu_0(1 - \eta^2)^{\frac{1}{2}}$. At the critical point $\Gamma_c = 2\nu_0(1 - \eta^2)^{\frac{1}{2}}$, all eigenvalues become degenerate, and all corresponding eigenmodes coalesce, resulting in an exceptional point of order $N+1$. In the reciprocal system ($\eta = 0$), the system reaches the exceptional point for $\Gamma_c = 2\nu_0$. To attain the exceptional point by enhancing non-reciprocity, it is necessary to minimize the system's dissipation such that at the unidirectional beam splitter ($\eta = 1$), dissipation is completely eliminated. Fig. 2 shows the eigenvalues as a function of the loss parameter Γ for $\omega_0 = \nu_0 = 1\,\mathrm{cm}^{-1}$ and $N = 4$ [34–36]. In Fig. 2a we set the non-reciprocity $\eta = 0$, representing a reciprocal beam splitter [26]. As the dissipation coefficient Γ increases, the real part of the eigenvalues exhibits level attraction and becomes degenerate at $\Gamma_c = 2\nu_0$, remaining constant thereafter. Conversely, the imaginary parts of the eigenvalues are identical and grow linearly with Γ for $\Gamma < \Gamma_c$, and become non-degenerate for $\Gamma > \Gamma_c$ [26]. As depicted in Fig. 2b, increasing the system's non-reciprocity, as predicted analytically, reduces the critical dissipation value required to reach an exceptional point.

Fig. 2c shows a unidirectional waveguide beam splitter, where the real parts of the eigenvalues remain uniform and unaffected by dissipation, while the imaginary parts of the eigenvalues increase linearly with Γ.

The non-reciprocal waveguide beam splitter offers an additional degree of flexibility for achieving higher-order exceptional points by modulating the non-reciprocity across the system. For any dissipation value within the range $\Gamma \in [0, 2\nu_0]$, higher-order exceptional points occur when the non-reciprocity parameter η is set to $\eta_c = \sqrt{4\nu_0^2 - \Gamma^2}/2\nu_0$. Fig. 3 illustrates the flow of eigenvalues as a function of the non-reciprocal parameter for different dissipation values, namely $\Gamma = 0$, 1.7, and 2 in plots (a), (b), and (c), respectively. Moreover, we provide a visual representation of the effect of the non-reciprocal and loss parameters on the exceptional point by calculating the expectation values of three spin-projection components $J_{\alpha,r} = \langle\lambda_r|\,\hat{J}_\alpha\,|\lambda_r\rangle$, $\alpha \in \{x, y, z\}$, in which $|\lambda_r\rangle$ is a complex eigenvector of the Hamiltonian (4). Figure 4 presents the evolution of these components for varying loss parameter Γ and nonreciprocal parameter η for $N = 4$ photon subspaces. Each subplot represents a distinct combination of disssipation and non-reciprocity, demonstrating their effect on the eigenmode. In the top row (a–c), the system remains reciprocal ($\eta = 0$), showing how increasing Γ affects the spin projections. At $\Gamma = 0.75\ \Gamma_c$, the spin projections lie in the $x - y$ plane, see the plot (a); if Γ reaches the exceptional point Γ_c, the eigenvectors coalesce, as demonstrated by the plot (b), signifying the system's transition through the exceptional point. As dissipation increases beyond this critical value, the eigenvalues are located in the $y - z$ plane, see plot (c). In the middle row (d–f), the system incorporates intermediate non-reciprocity $\eta = \eta_c = 0.661$. Notably, in panel (d), the system reaches the exceptional point at a lower dissipation value $\Gamma = 0.75\ \Gamma_c$, indicating that the presence of non-reciprocity allows the system to transition through the exceptional point earlier than in the reciprocal case. This demonstrates how non-reciprocity effectively lowers the threshold for reaching the exceptional point.

In the bottom row (g–i), the system is fully unidirectional ($\eta = 1$), hence non-reciprocity dominates the system dynamics. Unlike the previous cases, where the system transitions to the exceptional point at specific loss values, here the system has already reached the exceptional point in a lossless regime ($\Gamma = 0$). Consequently, the variations in dissipation beyond this point no longer induce a significant structural change in the spin-projections. This is reflected in the fact that the three plots (g–i) appear nearly identical, indicating that the spin projections remain robust even as dissipation increases. This confirms that in a unidirectional system, the exceptional point is dictated primarily by non-reciprocity rather than loss, leading to a saturation effect where further dissipation does not significantly alter the eigenmode structure.
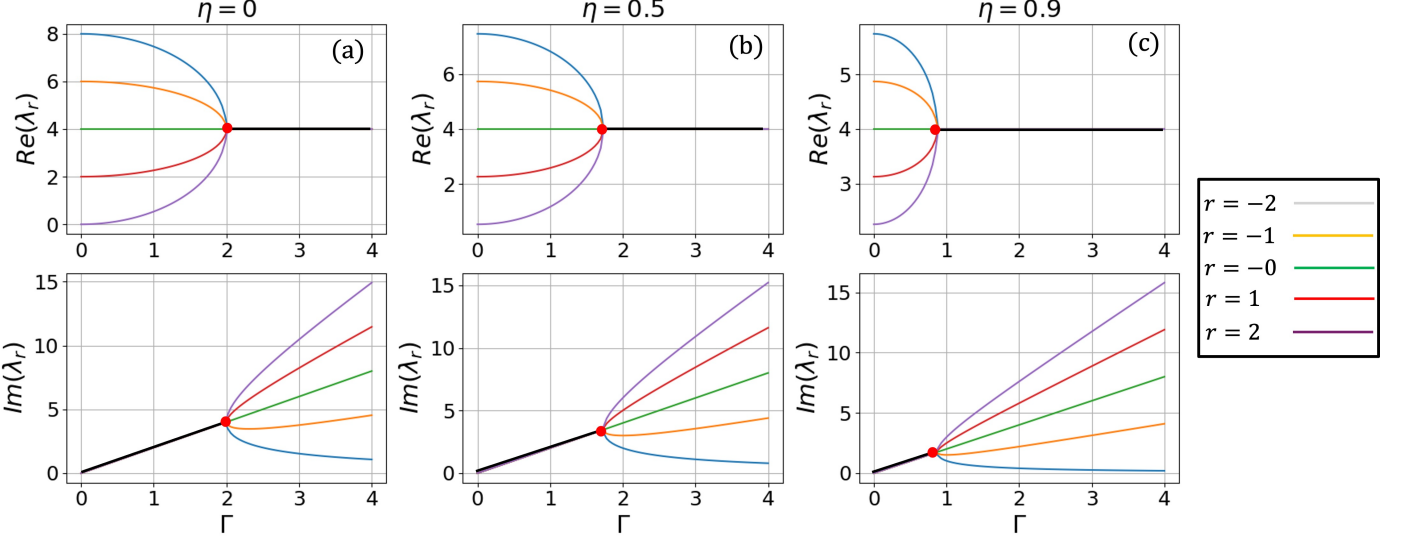
FIG. 2. Real and Imaginary parts of the eigenvalues λ_r of the Hamiltonian in Eq. (4) (with $\omega_0 = \nu_0 = 1\,\mathrm{cm}^{-1}$ in Eqs. (4), (14)) vs. the dissipation constant Γ for $N = 4$ with (a) $\eta = 0$ (reciprocal), (b) $\eta = 0.8$ and (c) $\eta = 1$ (unidirectional). The system reaches the exceptional point (EP of order five) at $\Gamma_c = 2\nu_0(1 - \eta^2)^{\frac{1}{2}}$.
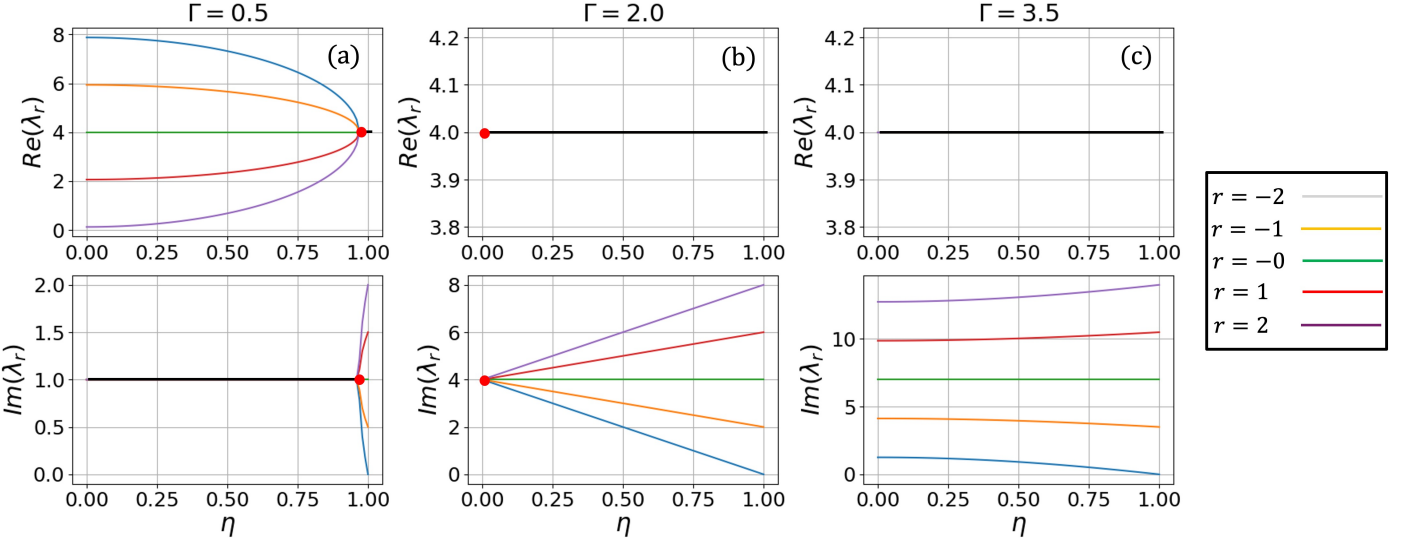

FIG. 3. Flow of eigenvalues λ_r of the Hamiltonian in Eq. (4) for $N = 4$ as a function of the non-reciprocity parameter η with dissipation values (a) $\Gamma = 0$ (lossless), (b) $\Gamma = 1.7$ and (c) $\Gamma = 2\nu_0$. The system reaches the higher-order exceptional points (EPs of order five) by adjusting η to the critical value $\eta_c = \sqrt{4\nu_0^2 - \Gamma^2}/2\nu_0$.

III. DYNAMICS OF THE NON-RECIPROCAL BEAM SPLITTER

In this section, we explore the dynamics of the lossy non-reciprocal beam splitter. The goal is to find the behavior of the intensity $I(z)$ within the N-photon subspace as a function of the propagation distance z in the waveguide. Since the waveguide is homogeneous in z-direction, and since we use units such that the

propagation velocity v in the waveguide is $v = 1$, the behavior $I(z)$ directly corresponds to the time evolution of the intensity $I(t)$ as a function of time t at a fixed position in the waveguide. To obtain a photon-number-resolved population, we need to find the time evolution operator $\hat{\mathcal{G}}(z)$ for a 2-leg lossy beam splitter satisfying the Schrödinger equation (identifying the propagation distance z in the waveguide with time,
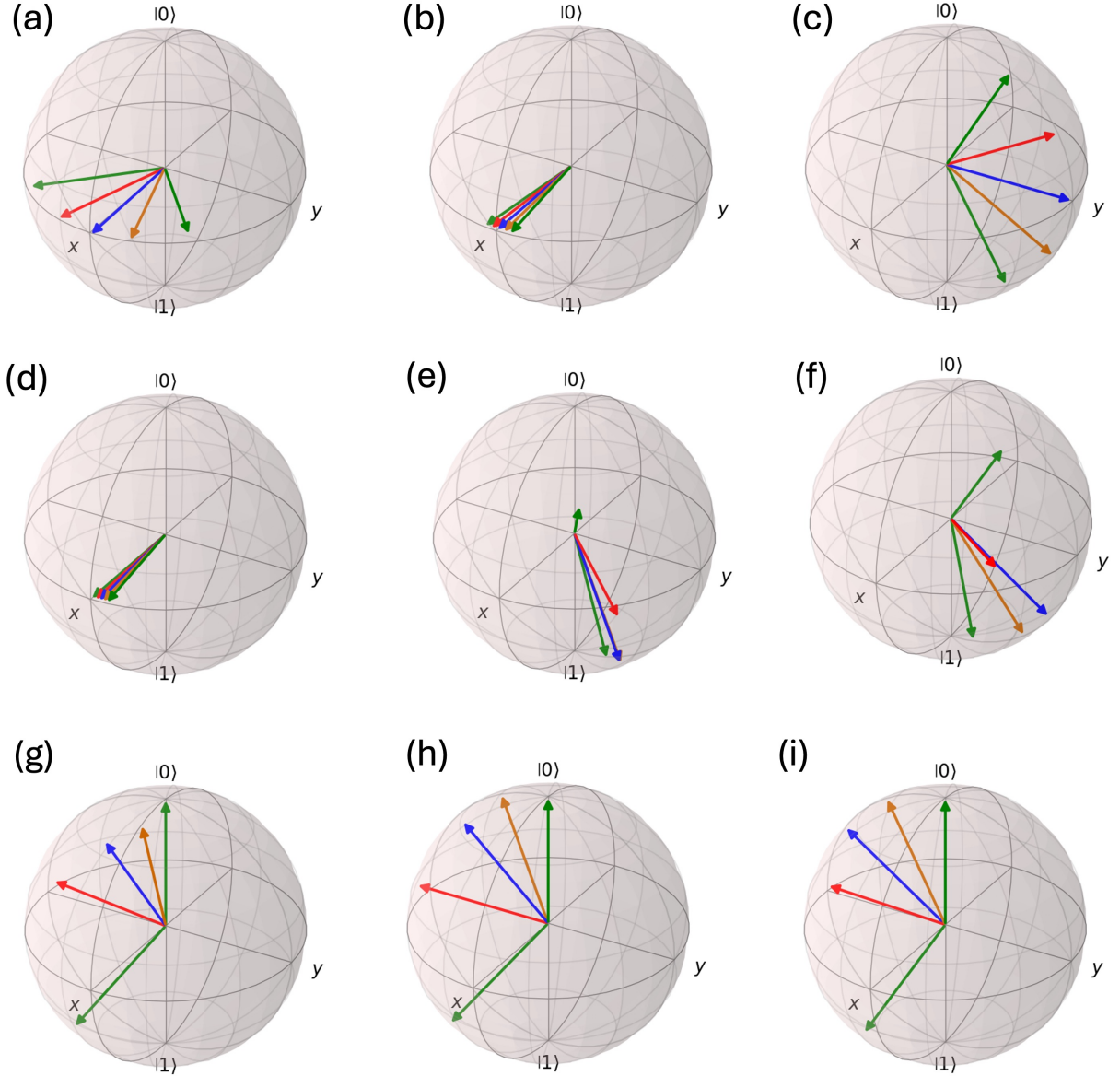
FIG. 4. Progression of the spin-projection components $\hat{J}_{x,y,z}$ for $N + 1$ eigenmodes $|\lambda_r\rangle$ where we consider $N = 4$ photons. In our diagrams we choose the following values of the dissipation Γ and non-reciprocity η: (a) $\Gamma = 0.75\ \Gamma_c$, $\eta = 0$, (b) $\Gamma = \Gamma_c$, $\eta = 0$, (c) $\Gamma = 1.5\ \Gamma_c$, $\eta = 0$, (d) $\Gamma = 0.75\ \Gamma_c$, $\eta = \eta_c = 0.661$, (e) $\Gamma = \Gamma_c$, $\eta = \eta_c$, (f) $\Gamma = 1.5\ \Gamma_c$, $\eta = \eta_c$, (g) $\Gamma = 0.75\ \Gamma_c$, $\eta = 1$, (h) $\Gamma = \Gamma_c$, $\eta = 1$, (i) $\Gamma = 1.5\ \Gamma_c$, $\eta = 1$.

see the remark above)

$$i\partial_z \hat{\mathcal{G}}(z) = \hat{H}\hat{\mathcal{G}}(z). \tag{16}$$

To find the solution of Eq. (16) we use the Wei-Norman method [37, 38] to express the time evolution in terms of SU(2) operators $\hat{J}_\pm$, $\hat{J}_z$ and the total number operator $\hat{N}$. It is given by

$$\hat{\mathcal{G}}(z) = e^{-i(\omega_0 - i\Gamma/2)\hat{N}z} e^{-if_+(z)\hat{J}_+} e^{-if_z(z)\hat{J}_z} e^{-if_-(z)\hat{J}_-}. \tag{17}$$

By substituting the time-evolution operator $\hat{\mathcal{G}}(z)$ into the Schrödinger equation, one can show that the three complex-valued functions $f_\pm(z)$ and $f_z(z)$ satisfy the following set of coupled, nonlinear differential equations:

$$\partial_z f_- = \nu' e^{-if_z}, \tag{18}$$
$$\partial_z f_+ = \nu + \nu' f_+^2 - \Gamma f_+, \tag{19}$$
$$\partial_z f_z = -i\Gamma + 2i\nu' f_+. \tag{20}$$

The analytical solutions to these three nonlinear equations for the initial condition $G(0) = 0$, equivalent

to $f_\pm(0) = f_z(0) = 0$, are expressed as follows:

$$f_z(z) = -2i \ln \left[\cos(z\Delta\lambda/2) + \frac{\Gamma}{\Delta\lambda} \sin(z\Delta\lambda/2) \right],$$

$$f_+(z) = \frac{\Gamma}{2\nu'} + \frac{\Delta\lambda}{2\nu'} \left[\frac{\tan(z\Delta\lambda/2) - \frac{\Gamma}{\Delta\lambda}}{1 + \frac{\Gamma}{\Delta\lambda}\tan(z\Delta\lambda/2)} \right],$$

$$f_-(z) = \frac{\Gamma}{2\nu} + \frac{\Delta\lambda}{2\nu} \left[\frac{\tan(z\Delta\lambda/2) - \frac{\Gamma}{\Delta\lambda}}{1 + \frac{\Gamma}{\Delta\lambda}\tan(z\Delta\lambda/2)} \right]. \quad (21)$$

The functions $f_\pm$ are real, irrespective of whether the system passes through an exceptional point, but $f_z(z)$ is complex in general. Note that unlike the case of a reciprocal beam splitter, here $f_+(z) \neq f_-(z)$, reflecting the non-reciprocal nature of the system.

If the system approaches a unidirectional regime, i.e., $1 - \eta := \epsilon \ll 1$, then the f-functions can be expanded as

$$f_z(z) = -i\Gamma z - \frac{4i\nu_0^2(1 - e^{-\Gamma z} - z\Gamma)\epsilon}{\Gamma^2} + \mathcal{O}(\epsilon^2),$$

$$f_+(z) = \frac{2\nu_0^3}{\Gamma}(1 - e^{-\Gamma z})\epsilon^2 + \mathcal{O}(\epsilon^3),$$

$$f_-(z) = \frac{4\nu_0^3}{\Gamma}(1 - e^{-\Gamma z})\epsilon + \mathcal{O}(\epsilon^2). \quad (22)$$

Thus, for $\epsilon \to 0$, corresponding to the unidirectional limit $\eta \to 1$, f_+ approaches zero more rapidly than the other f-functions. When the system reaches the unidirectional regime, the only significant contribution to the time evolution is $f_z(z)$, which simplifies to a linear dependence on the dissipation rate.

To investigate the dynamics of the non-reciprocal waveguide beam splitter, we examine the evolution of a NOON-state, defined as the initial state

$$|\text{NOON}\rangle = |\psi(0)\rangle = \frac{|N\rangle_a |0\rangle_b + |0\rangle_a |N\rangle_b}{\sqrt{2}}, \quad (23)$$

where $|N\rangle_a$ and $|N\rangle_b$ represent the N-photon states in the respective modes a and b. To analyze the system's evolution, our numerical approach involves post-selecting a subset of the system's state space (manifold) corresponding to a specific quantum outcome. Specifically, for an N-photon input, we consider only those cases where the total number of photons detected is exactly N, and no photons are absorbed in the lossy waveguide. We consider the normalized, z-dependent occupation function

$$P(m; |\psi(z)\rangle) = \frac{|\langle m|\psi(z)\rangle|^2}{\langle\psi(z)|\psi(z)\rangle}, \quad (24)$$

which fulfill $\sum_{m=0}^{N} P(m; |\psi(z)\rangle) = 1$.

Figure 5 depicts the normalized mode occupation in Eq. (24) as a function of the propagation distance z for $N = 4$ (corresponding to the time evolution of the mode occupation at a fixed position in the waveguide,

see text above Eq. (16)), considering different values of the loss parameter and degrees of nonreciprocality. In the reciprocal regime, when the dissipation is below the exceptional point Γ_c, the mode occupation exhibits oscillatory behavior across the five modes, with energy transferring from regions of lowest occupation to highest occupation (Fig. 5a). At the exceptional point Γ_c, the mode occupation stabilizes, with energy accumulating in the low-loss region (Fig. 5b). This behavior persists when dissipation exceeds the critical value Γ_c (Fig. 5c). In the non-reciprocal regime and for low loss, where $\eta \neq 0$ and $\Gamma < \Gamma_c$, the periodic pattern is disrupted, and photons preferentially occupy higher-order modes (Fig. 5, parts (d) and (g)). However, in the non-reciprocal regime where $\Gamma \geq \Gamma_c$, the non-reciprocal parameter no longer plays a significant role, and photons do not occupy higher modes, as shown in Fig. 5, parts (e), (f), (h), and (i). These results emphasize the impact of nonreciprocity on the mode occupation dynamics, particularly in the low-dissipation regime. Beyond the exceptional point, however, the dispersion parameter Γ becomes dominant, effectively stabilizing the lower modes.

Figure 6 illustrates the dynamics of photon occupation for $N = 2$. The behavior of photon occupation follows a similar pattern to that observed in Fig. 5 for $N = 4$. Specifically, as the loss parameter increases from the left and surpasses the exceptional point, the photon occupation stabilizes, resembling the trends shown in Fig. 5. This stability occurs as the dissipation exceeds the exceptional point, leading to a stable energy distribution across the modes, analogous to the behavior seen in the corresponding plots for $N = 4$. Although the overall mode occupation dynamics for $N = 2$ resembles those observed for $N = 4$, the two-photon case holds particular importance due to the Hong-Ou-Mandel (HOM) effect [39–41]. In Hermitian systems, the HOM effect manifests itself as photon bunching, where two identical photons interfere destructively in certain modes, leading to their coalescence in the same output state. Notably, as indicated in Fig. 7, in the low-dispersion regime the HOM effect is observed. However, when the dispersion is equal to or greater than the exceptional point the HOM effect is no longer achievable.

IV. CONCLUSIONS

In this study, we have examined the eigenvalue spectrum and dynamics of a non-reciprocal, lossy waveguide beam splitter to uncover the mechanisms leading to higher-order exceptional points (EPs). By incorporating non-reciprocity as an additional degree of freedom, we demonstrated the feasibility of achieving $(N + 1)$-fold exceptional points without stringent requirements for dissipation.

Our analysis illustrates that non-reciprocity significantly influences the eigenvalue spectrum, with the critical dissipation required for EPs decreasing as
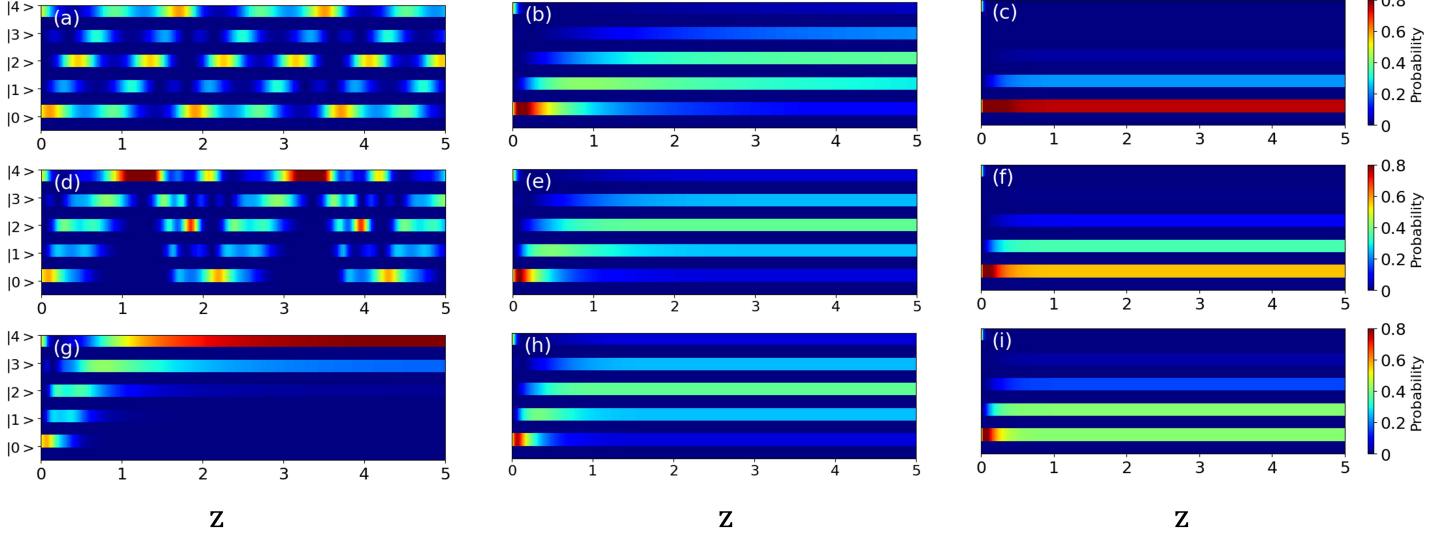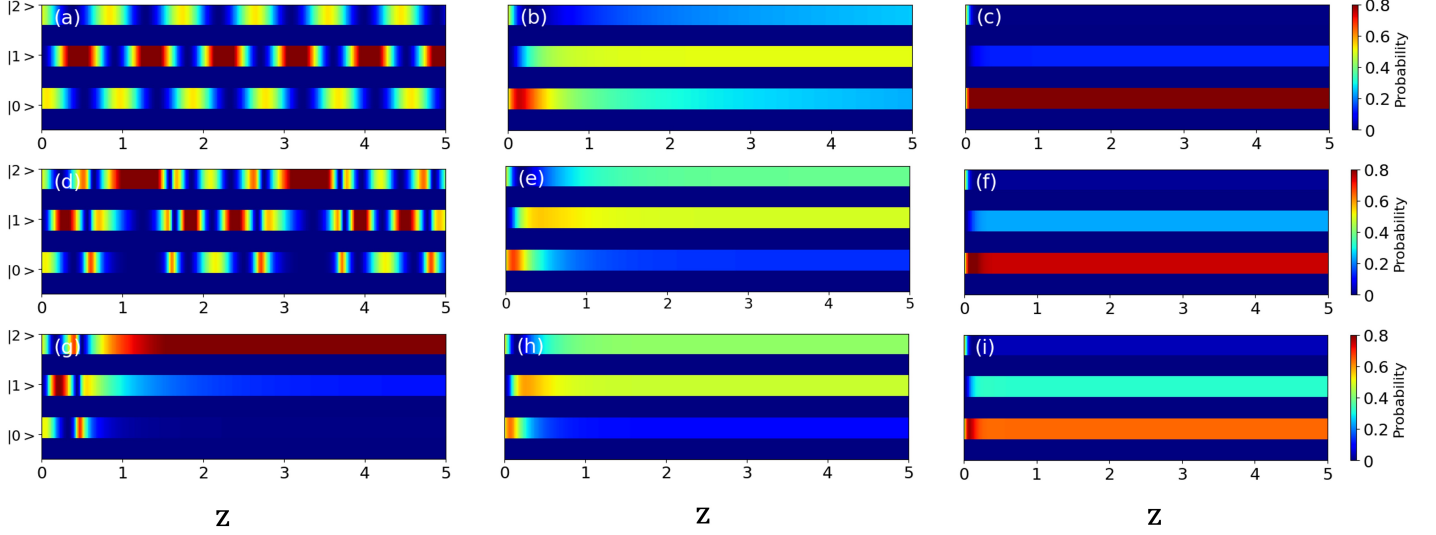
FIG. 5. Mode occupation dynamics for $N = 4$ photons for different dissipation and non-reciprocity. (a) $\Gamma = 0.25\ \Gamma_c, \eta = 0$, (b) $\Gamma = \Gamma_c, \eta = 0$, (c) $\Gamma = 2\Gamma_c, \eta = 0$, (d) $\Gamma = 0.25\ \Gamma_c, \eta = 0.5$, (e) $\Gamma = \Gamma_c, \eta = 0.5$, (f) $\Gamma = 2\ \Gamma_c, \eta = 0.5$, (g) $\Gamma = 0.25\ \Gamma_c, \eta = 1$, (h) $\Gamma = \Gamma_c, \eta = 1$ (i) $\Gamma = 2\ \Gamma_c, \eta = 1$.

FIG. 6. Mode occupation dynamics for $N = 2$ photons for different dissipation and non-reciprocity. (a) $\Gamma = 0.25\ \Gamma_c, \eta = 0$, (b) $\Gamma = \Gamma_c, \eta = 0$, (c) $\Gamma = 2\Gamma_c, \eta = 0$, (d) $\Gamma = 0.25\ \Gamma_c, \eta = 0.5$, (e) $\Gamma = \Gamma_c, \eta = 0.5$, (f) $\Gamma = 2\ \Gamma_c, \eta = 0.5$, (g) $\Gamma = 0.25\ \Gamma_c, \eta = 1$, (h) $\Gamma = \Gamma_c, \eta = 1$ (i) $\Gamma = 2\ \Gamma_c, \eta = 1$.

non-reciprocity increases. In the limiting case of a unidirectional system, exceptional points emerge even in the absence of dissipation, highlighting the potential of non-reciprocal waveguide beam splitters for robust sensing and precision measurement applications. Furthermore, our results for the eigenvector evolution offer valuable insight into the geometric and dynamical characteristics of systems near EPs, with spin projection components serving as an intuitive visualization of coalescing eigenstates. The results of this work emphasize the versatility of non-reciprocal platforms in engineering higher-order EPs, which hold promise for advanced interferometric systems [42], quantum state manipulation [43], and next-generation sensing technologies. Future research may extend this framework to nonlinear or time-dependent systems, potentially uncovering new regimes of EP-driven phenomena and expanding the applicability of non-Hermitian physics.
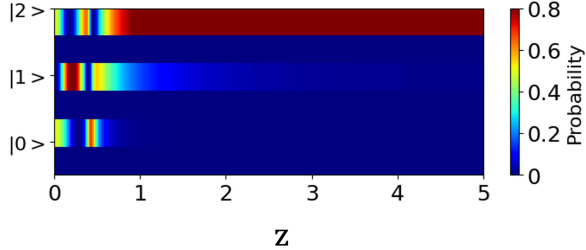
FIG. 7. Mode occupation dynamics for $N = 2$ photons at exceptional points ($\Gamma = 0, \eta = 1$), representing the HOM effect.

[1] V. M. Martinez Alvarez, J. E. Barrios Vargas, and L. E. F. Foa Torres, Non-hermitian robust edge states in one dimension: Anomalous localization and eigenspace condensation at exceptional points, Phys. Rev. B **97**, 121401 (2018).

[2] S. Yao and Z. Wang, Edge states and topological invariants of non-hermitian systems, Phys. Rev. Lett. **121**, 086803 (2018).

[3] H. Ghaemi-Dizicheh and H. Schomerus, Compatibility of transport effects in non-hermitian nonreciprocal systems, Phys. Rev. A **104**, 023515 (2021).

[4] H. Ghaemi-Dizicheh, Transport effects in non-hermitian nonreciprocal systems: General approach, Phys. Rev. B **107**, 125155 (2023).

[5] W. D. Heiss, Exceptional points of non-hermitian operators, Journal of Physics A: Mathematical and General **37**, 2455 (2004).

[6] W. D. Heiss, The physics of exceptional points, Journal of Physics A: Mathematical and Theoretical **45**, 444016 (2012).

[7] H. Xu, D. Mason, L. Jiang, and J. Harris, Topological energy transfer in an optomechanical system with exceptional points, Nature **537**, 80 (2016).

[8] G. Xu, X. Zhou, Y. Li, Q. Cao, W. Chen, Y. Xiao, L. Yang, and C.-W. Qiu, Non-hermitian chiral heat transport, Phys. Rev. Lett. **130**, 266303 (2023).

[9] Y. Xu, L. Li, H. Jeong, S. Kim, I. Kim, J. Rho, and Y. Liu, Subwavelength control of light transport at the exceptional point by non-hermitian metagratings, Science Advances **9**, eadf3510 (2023), https://www.science.org/doi/pdf/10.1126/sciadv.adf3510.

[10] S. Assawaworrarit, X. Yu, and S. Fan, Robust wireless power transfer using a nonlinear parity–time-symmetric circuit, Nature **546**, 387 (2017).

[11] J. Doppler, A. A. Mailybaev, J. Böhm, U. Kuhl, A. Girschik, F. Libisch, T. J. Milburn, P. Rabl, N. Moiseyev, and S. Rotter, Dynamically encircling an exceptional point for asymmetric mode switching, Nature **537**, 76 (2016).

[12] T. Goldzak, A. A. Mailybaev, and N. Moiseyev, Light stops at exceptional points, Phys. Rev. Lett. **120**, 013901 (2018).

[13] B. Peng, S. K. Özdemir, S. Rotter, H. Yilmaz, M. Liertzer, F. Monifi, C. M. Bender, F. Nori, and L. Yang, Loss-induced suppression and revival of lasing, Science **346**, 328 (2014), https://www.science.org/doi/pdf/10.1126/science.1258004.

[14] R. Thomas, H. Li, F. M. Ellis, and T. Kottos, Giant non-reciprocity near exceptional-point degeneracies, Physical Review A **94**, 043829 (2016).

[15] R. Thomas, H. Li, F. M. Ellis, and T. Kottos, Giant nonreciprocity near exceptional-point degeneracies, Phys. Rev. A **94**, 043829 (2016).

[16] J. Wiersig, Enhancing the sensitivity of frequency and energy splitting detection by using exceptional points: Application to microcavity sensors for single-particle detection, Phys. Rev. Lett. **112**, 203901 (2014).

[17] H. Hodaei, A. U. Hassan, S. Wittek, H. Garcia-Gracia, R. El-Ganainy, D. N. Christodoulides, and M. Khajavikhan, Enhanced sensitivity at higher-order exceptional points, Nature **548**, 187 (2017).

[18] W. Chen, Ş. Kaya Özdemir, G. Zhao, J. Wiersig, and L. Yang, Exceptional points enhance sensing in an optical microcavity, Nature **548**, 192 (2017).

[19] J. Zhang, B. Peng, Ş. K. Özdemir, K. Pichler, D. O. Krimer, G. Zhao, F. Nori, Y.-x. Liu, S. Rotter, and L. Yang, A phonon laser operating at an exceptional point, Nature Photonics **12**, 479 (2018).

[20] C. Wang, X. Jiang, G. Zhao, M. Zhang, C. W. Hsu, B. Peng, A. D. Stone, L. Jiang, and L. Yang, Electromagnetically induced transparency at a chiral exceptional point, Nature Physics **16**, 334 (2020).

[21] Y.-X. Xiao, J. Hu, Z.-Q. Zhang, and C. T. Chan, Experimental demonstration of splitting rules for exceptional points and their topological characterization, Phys. Rev. B **108**, 115427 (2023).

[22] Z. G. Yuto Ashida and M. Ueda, Non-hermitian physics,

Advances in Physics **69**, 249 (2020).

[23] M. H. Teimourpour, Q. Zhong, M. Khajavikhan, and R. El-Ganainy, Higher order exceptional points in discrete photonics platforms, in *Parity-time Symmetry and Its Applications*, edited by D. Christodoulides and J. Yang (Springer Singapore, Singapore, 2018) pp. 261–275.

[24] S. Dehdashti, R. Li, J. Liu, F. Yu, and H. Chen, Realization of non-linear coherent states by photonic lattices, AIP Advances **5** (2015).

[25] M. Setare, P. Majari, C. Noh, and S. Dehdashti, Photonic realization of the deformed dirac equation via the segmented graphene nanoribbons under inhomogeneous strain, Journal of Modern Optics **66**, 1663 (2019).

[26] M. A. Quiroz-Juárez, A. Perez-Leija, K. Tschernig, B. M. Rodríguez-Lara, O. S. Magaña-Loaiza, K. Busch, Y. N. Joglekar, and R. de J. León-Montiel, Exceptional points of any order in a single, lossy waveguide beam splitter by photon-number-resolved detection, Photon. Res. **7**, 862 (2019).

[27] L. Feng, R. El-Ganainy, and L. Ge, Non-hermitian photonics based on parity–time symmetry, Nature Photonics **11**, 752 (2017).

[28] M.-A. Miri and A. Alu, Exceptional points in optics and photonics, Science **363**, eaar7709 (2019).

[29] H. Ghaemi-Dizicheh and H. Ramezani, Non-hermitian floquet-free analytically solvable time-dependent systems, Opt. Mater. Express **13**, 678 (2023).

[30] T. Helbig, T. Hofmann, S. Imhof, M. Abdelghany, T. Kiessling, L. Molenkamp, C. Lee, A. Szameit, M. Greiter, and R. Thomale, Generalized bulk–boundary correspondence in non-hermitian topolectrical circuits, Nature Physics **16**, 747 (2020).

[31] D. Zou, T. Chen, W. He, J. Bao, C. H. Lee, H. Sun, and X. Zhang, Observation of hybrid higher-order skin-topological effect in non-hermitian topolectrical circuits, Nature Communications **12**, 7201 (2021).

[32] H. Ghaemi-Dizicheh, A class of stable nonlinear non-hermitian skin modes, Physica Scripta **99**, 125411 (2024).

[33] E. M. Graefe, U. Günther, H. J. Korsch, and A. E. Niederle, A non-hermitian symmetric bose–hubbard model: eigenvalue rings from unfolding higher-order exceptional points, Journal of Physics A: Mathematical and Theoretical **41**, 255206 (2008).

[34] G. Harder, T. J. Bartley, A. E. Lita, S. W. Nam, T. Gerrits, and C. Silberhorn, Single-mode parametric-down-conversion states with 50 photons as a source for mesoscopic quantum optics, Phys. Rev. Lett. **116**, 143601 (2016).

[35] L. Banchi, W. S. Kolthammer, and M. S. Kim, Multiphoton tomography with linear optics and photon counting, Phys. Rev. Lett. **121**, 250402 (2018).

[36] O. S. Magaña-Loaiza, R. d. J. León-Montiel, A. Perez-Leija, A. B. U'Ren, C. You, K. Busch, A. E. Lita, S. W. Nam, R. P. Mirin, and T. Gerrits, Multiphoton quantum-state engineering using conditional measurements, npj Quantum Information **5**, 80 (2019).

[37] J. Wei and E. Norman, Lie algebraic solution of linear differential equations, Journal of Mathematical Physics **4**, 575 (1963).

[38] S. Charzynski and M. Kun, Wei–norman equations for a unitary evolution, Journal of Physics A: Mathematical and Theoretical **46**, 265208 (2013).

[39] C. K. Hong, Z. Y. Ou, and L. Mandel, Measurement of subpicosecond time intervals between two photons by interference, Phys. Rev. Lett. **59**, 2044 (1987).

[40] R. J. Lewis-Swan, Proposal for demonstrating the hong–ou–mandel effect with matter waves, in *Ultracold Atoms for Foundational Tests of Quantum Mechanics* (Springer International Publishing, Cham, 2016) pp. 45–55.

[41] T. Jaouni, X. Gu, M. Krenn, A. D'Errico, and E. Karimi, Tutorial: Hong-ou-mandel interference with structured photons, arXiv preprint arXiv:2501.14961 (2025).

[42] J. Y. Lee, Unidirectional polarization beam splitter via an exceptional point and finite periodicity of non-hermitian $\mathcal{PT}$ symmetry, Phys. Rev. A **110**, 033521 (2024).

[43] K. Wang, L. Xiao, H. Lin, W. Yi, E. J. Bergholtz, and P. Xue, Experimental simulation of symmetry-protected higher-order exceptional points with single photons, Science Advances **9**, eadi0732 (2023), https://www.science.org/doi/pdf/10.1126/sciadv.adi0732.